Energy materials

CrossMark

Porous layer assembled hierarchical Co$_3$O$_4$ as anode materials for lithium-ion batteries

Ximei Zhai[1], Xiangming Xu[1], Xiaoliang Zhu[1], Yongjie Zhao[1,*], Jingbo Li[1], and Haibo Jin[1]

[1] Beijing Key Laboratory of Construction Tailorable Advanced Functional Materials and Green Applications, School of Materials Science and Engineering, Beijing Institute of Technology, Beijing 100081, China

ABSTRACT

The flower-like Co$_3$O$_4$ particles with three-dimensional structure have been achieved by inheriting the flower-like framework of β-Co(OH)$_2$ particles fabricated by a facile solvothermal method without any surfactant. The obtained Co$_3$O$_4$ microflower, which was composed of large amounts of self-assembled porous ultrathin nanosheets, exhibited excellent electrochemical performances in terms of high specific capacity and good cycle stability when being evaluated as anode materials for lithium-ion battery. Specifically, a high reversible capacity of above 1100 mA h g^{-1} was achieved after 50 cycles at the current density of 296 mA g^{-1}. Hierarchical flower-like structure with mesoporous was considered as providing more active sites for Li$^+$ insertion and paths for transport of Li$^+$, which led to faster lithium-ion diffusion. Co$_3$O$_4$ porous flower-like nanostructures possessed significant potential application in energy storage systems.

Introduction

On account of the merits of high energy density and long cycle life, lithium-ion batteries (abbreviated as LIB's) are widely applied as power supply in various electronic devices [1, 2]. In order to realize higher power density and longer life span, numerous efforts have been taken to develop novel and high-performance electrode materials [3–6]. One significant aspect to promote performances of batteries is synthesizing functional nanomaterials with controlled size and shape as electrode materials [7, 8].

Meanwhile, spinel cobalt oxide (Co$_3$O$_4$) has been extensively investigated as anode material in LIB's, due to its high theoretic capacity (890 mA h g^{-1}) [9]. As a result of its relative abundance and facile synthesis, Co$_3$O$_4$ is especially attractive for energy storage systems. However, the large volume variation of Co$_3$O$_4$ structure during the lithium uptake/release process severely reduces the stability and longevity of LIB's [10]. Different morphologies of Co$_3$O$_4$ nanostructures have been synthesized and researched, aimed at overcoming these drawbacks in their performances in LIB's [11]. Nanocages [12],

---

Ximei Zhai and Xiangming Xu have contributed equally to this study and share first authorship.

Address correspondence to E-mail: zhaoyjpeace@gmail.com

nanotubes [13], hollow nanostructures [14, 27–29] and so forth have been developed through different preparation methods, and their performances as anode materials have been researched systematically.

Recently, hierarchical flower-like microsphere with porous structure has attracted great attention after being prepared successfully. The three-dimensional hierarchical structure possessing large specific surface area offer more active sites for accessibility of the electrolyte and the fast ion diffusion in redox reactions [32, 34]. In this aspect, a great deal of porous Co_3O_4 nanoflowers which are assembled with nanorods [15], smooth nanosheets [16] and so forth with remarkable properties have been prepared and investigated [31, 33]. In this study, Co_3O_4 microflower assembled by ultrathin porous nanosheets was synthesized. The obtained hierarchical Co_3O_4 structure offered higher specific surface area and larger pore volume, which had access to extra interfacial reaction sites of Li^+ insertion on cycling. As a result, the Co_3O_4 anode material exhibited excellent electrochemical performances in Li-ion battery. Presumably, porous structures on these ultrathin nanosheets are the key in enhancing the LIB's performance.

Experimental

Preparation and characterization

3 mmol of $C_4H_6CoO_4 \cdot 4H_2O$ was dissolved in the mixed solvent (1, 2-propanediol/water = 20:20, volume ratio) to form a transparent pink solution after stirring for 30 min at room temperature. Ammonium Hydroxide ($NH_3 \cdot H_2O$) was used to keep the pH value at 10. This homogeneous solution was transferred into a Teflon-lined stainless steel auto clave and kept in an oven at 220 °C for 24 h. After being cooled down to ambient temperature, the red hydroxide precipitate was collected by centrifugation and washed with deionized water and ethanol for several times, then dried in a vacuum oven at 70 °C for 10 h. By annealing the precursor at 400 °C for 2 h in air, black Co_3O_4 powder was successfully obtained.

An X-ray diffractometer (XRD, D8/ADVANCE diffractometer) was used to characterize phase of these samples with Cu $K\alpha(\lambda = 1.5418$ Å) radiation. The morphology and microstructure were observed by the field emission scanning electron microscope

(SEM, Oberkochen, Germany, LEO-1530) and transmission electron microscope (TEM, JEM-2100F). Thermogravimetric (TG) analysis of thermal decomposition of precursors was performed on Thermogravimetric analyzer (N33-TG 209 F3).

Electrochemical measurements

The electrochemical performance of as-prepared Co_3O_4 sample was evaluated using the CR2032-type coin cells. As-prepared Co_3O_4 as active material was mixed with acetylene black (as conductive agent) and Poly (vinylidene fluoride) (as binder) at a weight ratio of 7:2:1. N-methyl-2-pyrrolidone was used as the solvent to make the dry mixed powder into mixture paste. Then the paste was coated uniformly on the copper foil to fabricate electrode. And the electrode was dried in a vacuum drying oven at 80 °C for 24 h to remove the absorbed water. The as-prepared copper foil was punched into round sheets with a diameter of 14 mm. The mass loading of the active materials is about 0.95–1.18 mg cm^{-2}. A metal lithium foil was utilized as the counter and reference electrodes and a polypropylene microporous film as the separator. The Co_3O_4/Li half-cells were made in a dry Ar-filled glovebox using 1 mol/L $LiPF_6$ (EC: DMC, 1: 1, in volume) as the electrolyte. Cyclic voltammetry and electrochemical impedance measurements (AC voltage of 5 mV amplitude, 10 kHz–10 mHz) were performed using an electrochemical workstation (CHI 660B, Shanghai Chenhua instrument Co., Ltd).The electrochemical performance of two-electrode coin-type cell was charged and discharged over a voltage range of 0–3 V versus Li/Li^+ electrode at room temperature on LAND batteries test system (Wuhan, China).

Results and discussion

The SEM images in Fig. 1 exhibited the showed morphologies of synthesized β-$Co(OH)_2$ pink powder. As showed in Fig. 1a, it could be easily figured out that the microparticles were mainly made up of flower-like microspheres with the diameter in of 20–60 μm. The SEM images and the inserted image clearly revealed the details of the ultrathin sheets in Fig. 1b. Their surfaces and edges were pretty smooth and the thickness was about 50 nm. All the features
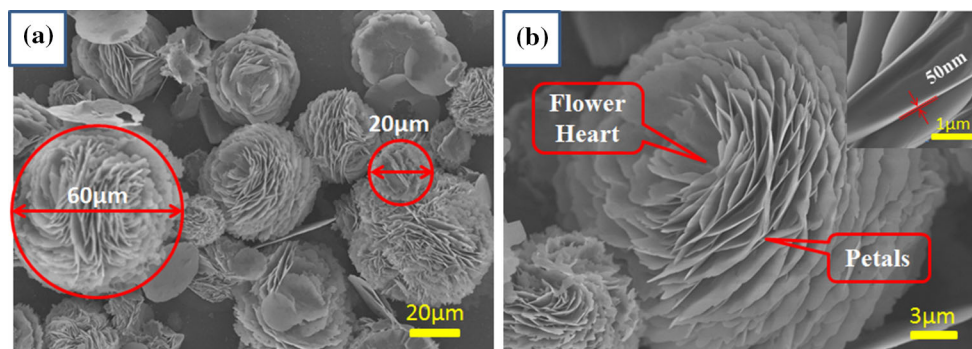
Figure 1 **a** Lower and **b** higher magnification SEM images of precursor.

mentioned above illustrated great surface properties of the as-synthesized β-Co(OH)$_2$ precursor.

For investigating the transformation from the as-synthesized β-Co(OH)$_2$ precursor to Co$_3$O$_4$, the Thermogravimetric analyzer (TG) and X-ray diffractometer (XRD) were employed to analyze the thermal decomposition behavior of precursor and the corresponding transformation of phase structure. Figure 2a depicted the TG curve of the precursor, which was identified as β-Co(OH)$_2$ by XRD pattern in Fig. 2c. According to the thermal decomposition process in Fig. 2a, three stages could be figured out. The weight loss before 160 °C in the first stage was about 3.3%, which was corresponding to the physical dehydration of the sample. The second stage came with the initial step of thermal decomposition from β-Co(OH)$_2$ to Co$_2$O$_3$, with about 86.3% weight left from 160 °C to 270 °C. As the temperature went higher toward 400 °C, the third stage which was the final thermal decomposition came with only 83.5% weight left, resulting in the final product Co$_3$O$_4$. And the XRD pattern in Fig. 2b of the sample after annealed at 400 °C for 2 h, well matched the standard spectrum of spinel Co$_3$O$_4$ (JCPDS Card No. 42-1467). Figure 2d showed FT-IR spectra of the precursor and Co$_3$O$_4$. Two strong absorptions at 659 and 562 cm^{-1} are ascribed to the decomposition of the hydroxide to Co$_3$O$_4$ [17]. The broad band at 495 cm^{-1} is assigned to Co–O. The peaks at 3421 and 1057 cm^{-1} are attributed to O–H stretching and C-O stretching vibrations of epoxy groups, respectively.

The morphology and microstructure of the obtained Co$_3$O$_4$ after annealing process were further characterized with SEM and TEM. Judging from SEM images with low magnification in Fig. 3a, b, it was found that the annealed products well preserved the flower-like framework of these precursors. However,

some interesting changes about the nanosheets happened, which could be figured out in the inserted images in Fig. 3b. Some mesoporous could be found clearly on these nanosheets. The porous nanosheets were further investigated via TEM, shown in Fig. 3c, d. The TEM image indicated that the mesoporous with different sizes uniformly distributed on nanosheets and the size of the mesoporous was far less than 50 nm. The SAED pattern inserted in Fig. 3c demonstrated the polycrystalline phase of spinel Co$_3$O$_4$. Besides, the d value with 0.29 nm of lattice plane in HRTEM image (Fig. 3d) matched well with (220) of spinel Co$_3$O$_4$.

To study the pore structure and the specific surface areas of the as-obtained Co$_3$O$_4$ nanostructures, nitrogen adsorption–desorption isotherms were carried out, and the corresponding results are showed in Fig. 4. The surface area and the average pore diameter are measured to be around 39.728 m^2/g and 23.74 nm, respectively. And the pore size distribution of Co$_3$O$_4$ is mainly located at 2–3 nm.

We investigated the electrochemical Li-ion charge and discharge behaviors of the Co$_3$O$_4$ powders by cyclic voltammetry (CV) in the voltage range of 0–3 V versus Li/Li$^+$. The CV curves of Co$_3$O$_4$ electrode for the first five cycles at a scan rate of 2.0 mV s^{-1} were shown in Fig. 5a. In the first cycle, the sharp cathodic peak at around 0.4 V was ascribed to the conversion reaction between Co$_3$O$_4$ and Li$^+$, relative to the formation of metallic Co and Li$_2$O [18]. The broad anodic peak at around 2.1 V was attributed to the delithiation reaction of Co$_3$O$_4$. In the subsequent cycles, the intensities of the cathodic peaks decreased, due to the irreversible reaction and the formation of a solid electrolyte interface (SEI) film at the interface between the electrolyte and nanostructured electrode [19].
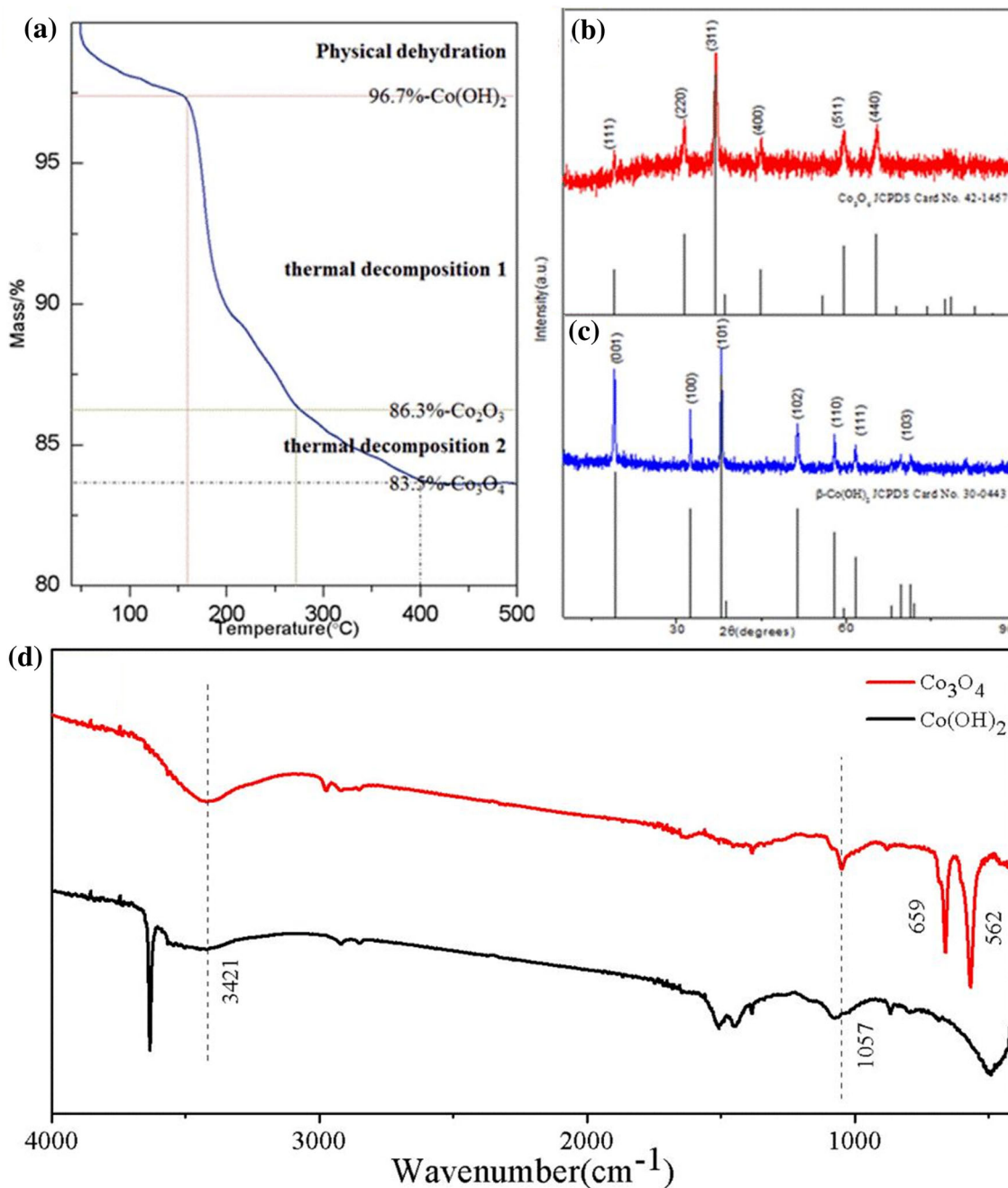
Figure 2 **a** TG curves of precursor, **b** XRD of sample annealing at 400 °C and the standard pattern of Co_3O_4, **c** XRD of precursor and the standard pattern of β-$Co(OH)_2$, **d** FT-IR spectra of β-$Co(OH)_2$ and Co_3O_4.

In Fig. 5b, the synthesized Co_3O_4 maintained the similar CV profiles when the scan rate increased from 0.2 to 1.0 mVs^{-1}. It proved that the flower-like Co_3O_4 had a fast CV response to the rapid potential scanning [20]. According to the CV profiles of different scanning speeds, we could find out the relationship of peak current and scan rate. The relationship of

peak current and scan rate could be expressed by a power law: $i = av^b$, where i is the current (A), a and b are arbitrary coefficients and v is the potential scan rate (V s^{-1}) [21, 22]. The coefficient b varies in the range 0.5 to 1, with a value of 0.5 being characteristic of a diffusion-limited process and a value of 1 for a capacitive process [23]. The relationship of peak
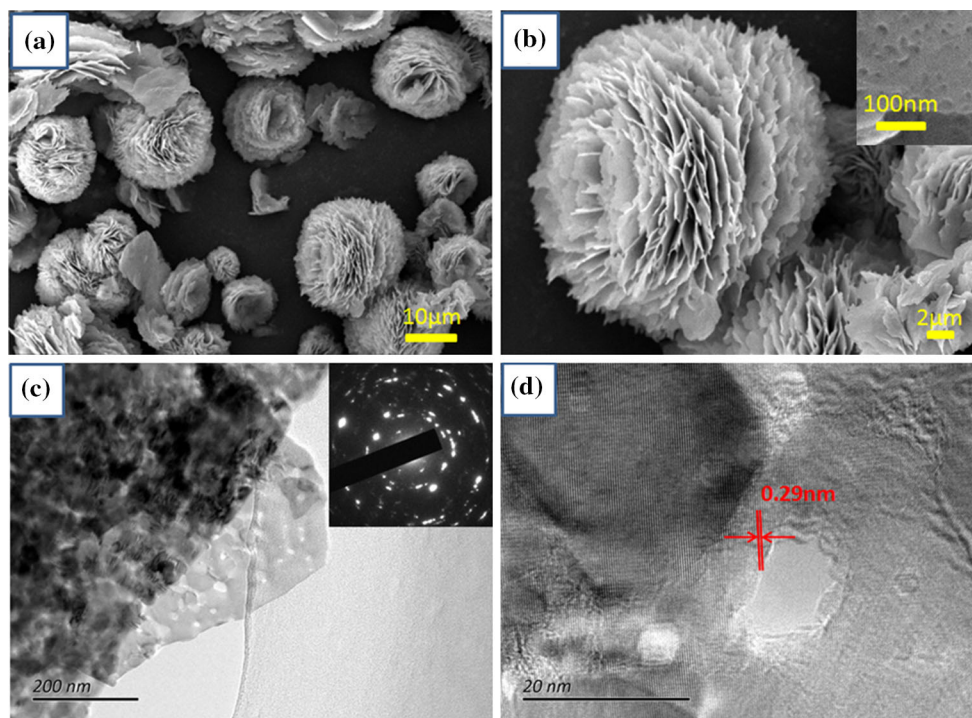
Figure 3 **a** and **b** LRSEM images of flower-like Co_3O_4 samples and the inserted HRSEM image of petal, **c** LRTEM image and SAED pattern of the obtained Co_3O_4 sample, **d** HRTEM image selected in red area in Fig. 3c.
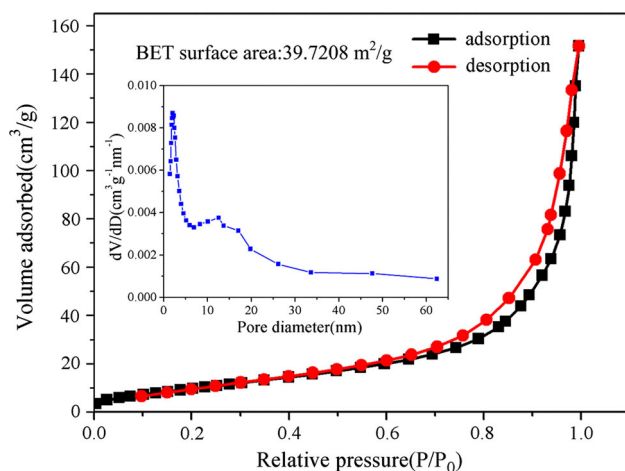

Figure 4 N_2 adsorption–desorption isotherm and pore-size-distribution curve (inset) of flower-like Co_3O_4.

current and scan rate in logarithmic algorithm was shown in Fig. 5c. The slope of the log (scan rate)-log (peak current) plots in cathodic and anodic processes are 0.863 and 0.885, respectively, indicating that the current is predominantly non-diffusion limited.

The electrochemical impedance spectroscopy (EIS) was used to evaluate the charge transfer and Li^+ diffusion kinetics of the synthesized Co_3O_4. Figure 5d showed there were two regions of an arc followed by

an inclined line of the Nyquist plot. The inclined line at low frequency represented the Warburg impedance, which was inversely proportional to the diffusion. The intercept at Z′-axis in high frequency represented the resistance of the electrolyte, which was relevant to the ohmic resistance [9]. And the diameter of the semicircle in the high-frequency region, which represented the interparticle contact resistance, was about 70 O, much smaller than the pristine Co_3O_4 electrode. It suggested that the contact and charge-transfer resistance of the synthesized Co_3O_4 electrode was lower [24].

Figure 6a displayed the cycling performance of the Co_3O_4 electrode at a current density of 296 mA g^{-1}. For comparison, we have listed the electrochemical performances of various Co_3O_4 nanostructures in Table 1. From Table 1, the hierarchical Co_3O_4 nanoflowers in this work exhibit the highest initial capacity. It was found that the initial discharge and charge capacities were 1685 and 1224 mA h g^{-1}, respectively, rendering an initial coulombic efficiency of 74.2%. The corresponding irreversible capacity loss might be mainly attributed to the formation of solid electrolyte interface (SEI) [25] and irreversible phase conversion of Co_3O_4 [26] during the first lithiation–
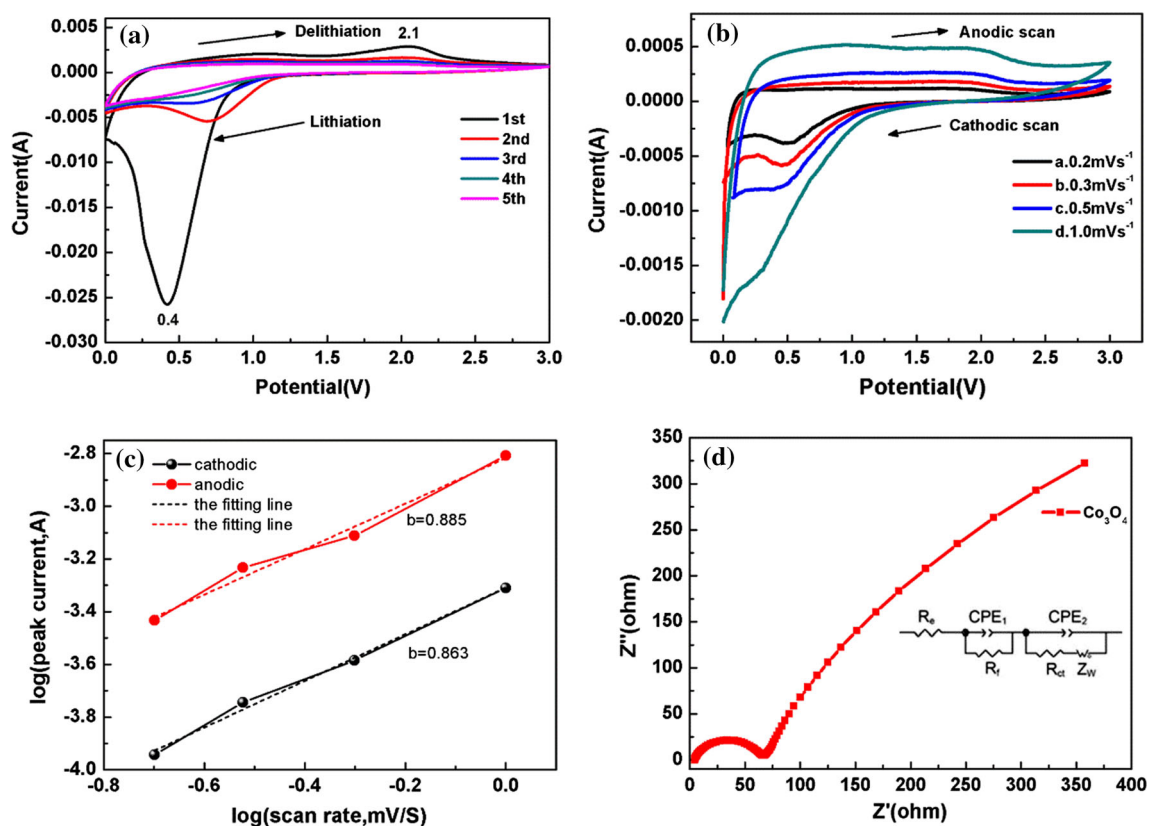
Figure 5 a CV curves within 5 cycles at scan rate of 2.0 mV s^{-1}, **b** cyclic voltammetry (CV) curves at different scan rates from 0.2 to 1.0 mV s^{-1}, **c** the relationship between peak current and scan rate, **d** the Nyquist plot of the sample with the inset showing the equivalent circuits.

delithiation cycle. Then the coulombic efficiency still maintained about 95% efficiency within 50 cycles. The charge and discharge capacities still kept above 1100 mA h g^{-1} within 50 cycles, higher than the theoretic capacity of bulk Co$_3$O$_4$ (about 890 mA h g^{-1}).This might be the reason of flower-like Co$_3$O$_4$ with mesoporous structure, which had more interfacial bonding for extra active sites of Li$^+$ insertion. It has been reported that the comparatively appropriate pore size was more convenient for the intercalation of Li$^+$ ions into the active materials, benefiting for its charge–discharge performance consequently [7]. Figure 6b revealed the representative discharge–charge curves of 1st, 2nd, 3rd, 10th and 50th of the electrode, which was in accordance with the cycling performance in Fig. 6a. The potential window was 0–3 V at a current density of 296 mA g^{-1}.

The rate capability of the Co$_3$O$_4$ electrode at higher current densities (445 and 890 mA g^{-1}) was shown in Fig. 6c. The initial capacity loss at a current density of 445 and 890 mA g^{-1} might have the same reasons with

that of 296 mA h g^{-1}. The discharge specific capacity at 445 mA g^{-1} began with 937 mA h g^{-1} at the second cycle, coming with a decay to about 690 mA h g^{-1} at the 50th cycle. While the current density was up to 890 mA g^{-1}, it began with about 831 mA h g^{-1} at the second cycle followed by a rapid decline to about 350 mA h g^{-1} after 30 cycles This might be attributed to the microstructure changes of Co$_3$O$_4$ active material. However, rate capability kept steady at the capacity of around 350 mA h g^{-1} and the coulombic efficiency could remain 98.5% after 30 cycles. It suggested that the electrode/electrolyte interface might approach to a more stable state gradually [7]. Figure 6d showed that the charge and discharge process with higher current density caused great reduction in rate capacity. The reason why the capacity reduced in the charge and discharge processes is that some of the extra sites were irreversible for Li$^+$. More inactive Li$^+$ were amassed in the anode material to form SEI layer when the current density got higher. Also, the pulverization of the structure got worse.
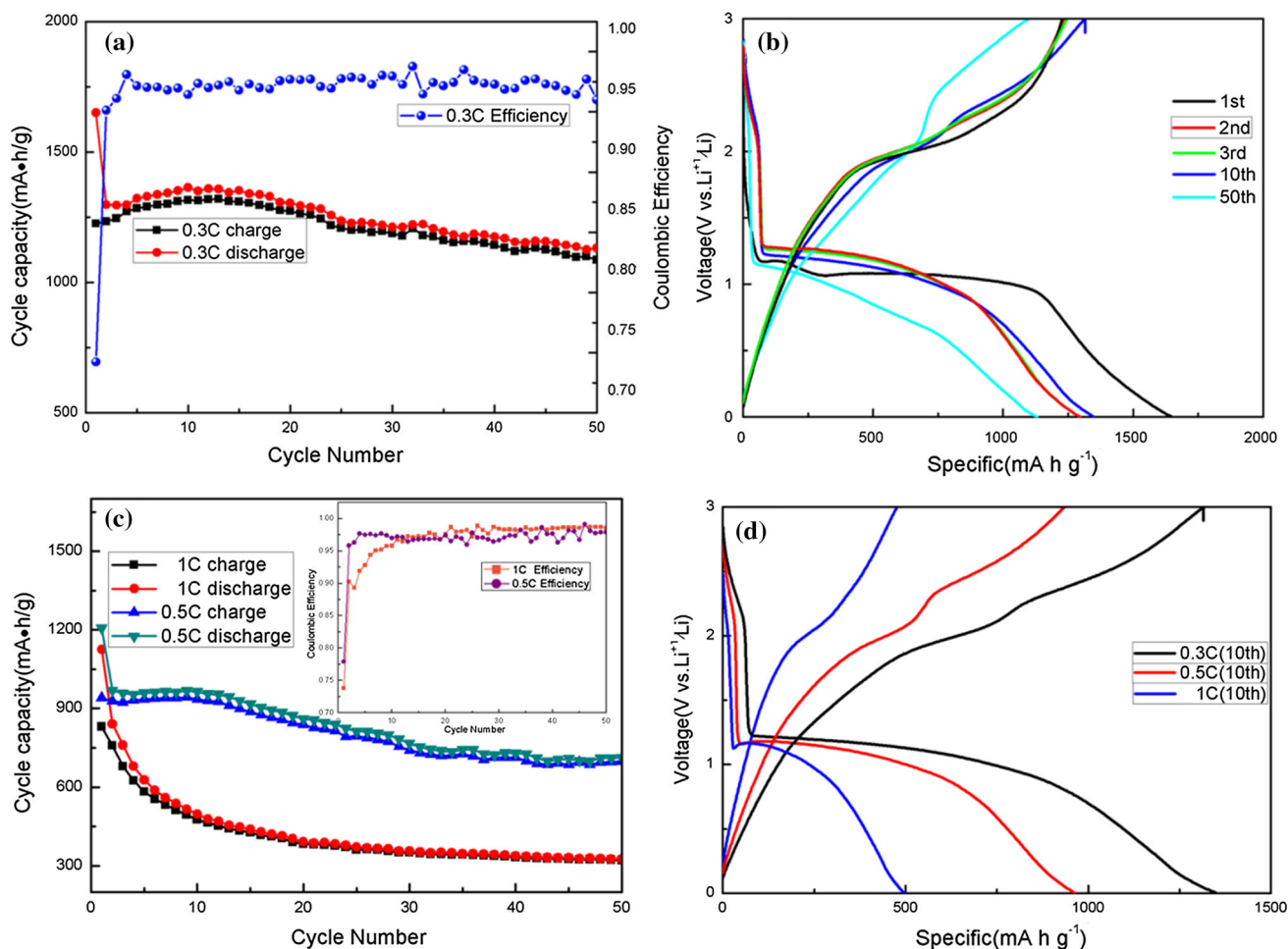
Figure 6 a Cycling performance of Co_3O_4 electrode at current densities of 296 mA g^{-1}, **b** the charge–discharge curves of the Co_3O_4 electrode in the voltage range of 0–3 V versus Li$^+$/Li at a current density of 296 mA g^{-1}, **c** the cycling performance of the Co_3O_4 electrode at current densities of 445 and 890 mA g^{-1}, **d** the charge–discharge curves of the Co_3O_4 electrode at a current density of 296,445 and 890 mA g^{-1}.

Table 1 Comparison of electrochemical performance of Co_3O_4 as anode material for the LIB

Materials	Current density (mAg^{-1})	Initial charge specific capacity (mA h g^{-1})	References
Co_3O_4 nanoparticles	100	900	[20]
Co_3O_4 nanosheets	150	1031	[30]
Hairy ball-like Co_3O_4	100	1200	[19]
Hierarchical Co_3O_4 nanoflowers	296	1224	This work

Conclusions

In summary, the Co_3O_4 microflower has been prepared by the hydrothermal method followed with annealing process. These hierarchical Co_3O_4 porous structures provide space for the large volume variation of Co_3O_4 structure during the lithium uptake/release process, preventing it from structure collapsing too quickly. The mesoporous structures provided the passageway for transport of Li$^+$ and more interfacial bonding for extra active sites of Li$^+$ insertion. The reversible capacity at 296 mA g^{-1} still kept above 1100 mA h g^{-1} after 50 cycles, suggesting Co_3O_4 with microflower structure is a promising anode material for LIBs.

Acknowledgements

References

[1] Tarascon JM, Armand M (2001) Issues and challenges facing rechargeable lithium batteries. Nature 414(6861):359–367

[2] Armand M, Tarascon JM (2008) Building better batteries. Nature 451(7179):652–657

[3] Wang J, Zhang Q, Li X, Xu D, Wang Z, Guo H, Zhang K (2014) Three-dimensional hierarchical Co_3O_4/CuO nanowire heterostructure arrays on nickel foam for high-performance lithium ion batteries. Nano Energy 6:19–26

[4] Ding C, Zhao Y, Yan D, Zhao Y, Zhou H, Li J, Jin H (2016) An insight into the convenience and efficiency of the freeze-drying route to construct 3D graphene-based hybrids for lithium-ion batteries. Electrochim Acta 221:124–132

[5] Zhao Y, Yan D, Ding C, Su D, Ge Y, Zhao Y, Zhou H, Li J, Jin H (2016) Fe_2O_3 nanocubes exposed (012) active facets combination with graphene rendering enhanced lithium storage capability. J Power Sources 327:658–665

[6] Ding C, Yan D, Zhao Y, Zhao Y, Zhou H, Li J, Jin H (2016) A bubble-template approach for assembling Ni–Co oxide hollow microspheres with an enhanced electrochemical performance as an anode for lithium ion batteries. Phys Chem Chem Phys 18(37):25879–25886

[7] Wu X, Wu W, Wang K, Chen W, He D (2015) Synthesis and electrochemical performance of flower-like $MnCo_2O_4$ as an anode material for sodium ion batteries. Mater Lett 147:85–87

[8] Xia Y, Xiong Y, Lim B, Skrabalak S (2009) Shape-controlled synthesis of metal nanocrystals: simple chemistry meets complex physics. Angew Chem Int Ed 48(1):60–103

[9] Fang D, Li L, Xu W, Li G, Li G, Wang N, Luo Z, Xu J, Liu L, Huang CL, Liang C (2013) Self-assembled hairy ball-like Co_3O_4 nanostructures for lithium ion batteries. J Mater Chem A 1:13203–13208

[10] Kong D, Luo J, Wang Y, Ren W, Yu T, Luo Y, Yang Y, Cheng C (2014) Three-dimensional Co3O4@MnO2 hierarchical nanoneedle arrays: morphology control and electrochemical energy storag. Adv Funct Mater 24(24):3815–3826

[11] Wang D, Wang Q, Wang T (2011) Morphology-controllable synthesis of cobalt oxalates and their conversion to mesoporous Co_3O_4 nanostructures for application in supercapacitors. Inorg Chem 50(14):6482–6492

[12] Yan N, Hu L, Li Y, Wang Y, Zhong H, Hu X, Kong X, Chen Q (2012) Co_3O_4 nanocages for high-performance anode material in lithium-ion batteries. J Phys Chem C 116(12):7227–7235

[13] Zhuo L, Wu Y, Ming J, Wang L, Yu Y, Zhang X, Zhao F (2013) Facile synthesis of a Co_3O_4–carbon nanotube composite and its superior performance as an anode material for Li-ion batteries. J Mater Chem A 1(4):1141–1147

[14] Wang Z, Zhou L (2012) Metal oxide hollow nanostructures for lithium-ion batteries. Adv Mater 24(14):1903–1911

[15] Yan C, Chen G, Zhou X, Sun J, Lv C (2016) Template-based engineering of carbon-doped Co3O4 hollow nanofibers as anode materials for lithium-ion batteries. Adv Funct Mater 26(9):1428–1436

[16] Liu J, Kelly SJ, Epstein ES, Pan Z, Huang X, Liu J, Braun PV (2015) Three-dimensionally scaffolded Co_3O_4 nanosheet anodes with high rate performance. J Power Sources 299:40–48

[17] Wang HW, Hu ZA, Chang YQ, Chen Y, Zhang Z, Yang Y, Wu H (2011) Preparation of reduced graphene oxide/cobalt oxide composites and their enhanced capacitive behaviors by homogeneous incorporation of reduced graphene oxide sheets in cobalt oxide matrix. Mater Chem Phys 130(1):672–679

[18] Park JS, Cho JS, Kim JH, Choi YJ, Kang YC (2016) Electrochemical properties of micron-sized Co_3O_4 hollow powders consisting of size controlled hollow nanospheres. J Alloys Compd 689:554–563

[19] Zhang XX, Xie QS, Yue GH, Zhang Y, Zhang XQ, Lu AL, Peng DL (2013) A novel hierarchical network-like Co_3O_4 anode material for lithium batteries. Electrochim Acta 111:746–754

[20] Zhao Y, Li Y, Ma C, Shao Z (2016) Micro-/nano-structured hybrid of exfoliated graphite and Co_3O_4 nanoparticles as high-performance anode material for Li-ion batteries. Electrochim Acta 213:98–106

[21] Lindström H, Södergren S, Solbrand A, Rensmo H, Hjelm J, Hagfeldt A, Lindquist S-T (1997) Li^+ ion insertion in TiO_2 (anatase). 2. Voltammetry on nanoporous films. J Phys Chem B 101(39):7717–7722

[22] Lübke M, Shin J, Marchand P, Brett D, Shearing P, Liu Z, Darr JA (2015) Highly pseudocapacitive Nb-doped TiO_2 high power anodes for lithium-ion batteries. J Mater Chem A 3:22908–22914

[23] Lübke M, Sumboja A, Johnson ID, Brett D, Shearing P, Liu Z, Darr JA (2016) High power nano-Nb_2O_5 negative electrodes for lithium-ion batteries. Electrochim Acta 192:363–369

[24] Pan L, Zhao H, Shen W, Dong X, Xu J (2013) Surfactant-assisted synthesis of a Co_3O_4/reduced graphene oxide

composite as a superior anode material for Li-ion batteries. J Mater Chem A 1(24):7159–7166

[25] Zhu X, Ning G, Ma X, Fan Z, Xu C, Gao J, Xu C, Wei F (2013) High density Co_3O_4 nanoparticles confined in a porous graphene nanomesh network driven by an electrochemical process: ultra-high capacity and rate performance for lithium ion batteries. J Mater Chem A 1(44):14023–14030

[26] Wang Y, Yan F, Liu SW, Tan AYS, Song H, Sun XW, Yang HY (2013) Onion-like carbon matrix supported Co_3O_4 nanocomposites: a highly reversible anode material for lithium ion batteries with excellent cycling stability. J Mater Chem A 1(17):5212–5216

[27] Wang J, Yang N, Tang H, Dong Z, Jin Q, Yang M, Kisailus D, Zhao H, Tang Z, Wang D (2013) Accurate control of multishelled Co_3O_4 hollow microspheres as high-performance anode materials in lithium-ion batteries. Angew Chem 125(25):6545–6548

[28] Li H, Ma H, Yang M, Wang B, Shao H, Wang L, Yu R, Wang D (2017) Highly controlled synthesis of multi-shelled NiO hollow microspheres for enhanced lithium storage properties. Mater Res Bull 87:224–229

[29] Zhang J, Ren H, Wang J, Qi J, Yu R, Wang D, Liu Y (2016) Engineering of multi-shelled SnO_2 hollow microspheres for highly stable lithium-ion batteries. J Mater Chem A 4(45):17673–17677

[30] Fan Y, Shao H, Wang J, Liu L, Zhang J, Cao C (2011) Synthesis of foam-like freestanding Co_3O_4 nanosheets with enhanced electrochemical activities. Chem Commun 47(12):3469–3471

[31] Zhao Y, Xu X, Zhao Y, Zhou H, Li J, Jin H (2016) Synthesis and their physicochemical behaviors of flower-like Co_3O_4 microspheres. J Alloys Compd 654:523–528

[32] Ding C, Su D, Ma W, Zhao Y, Yan D, Li J, Jin H (2017) Design of hierarchical CuS/graphene architectures with enhanced lithium storage capability. Appl Surf Sci 403:1–8

[33] Xu X, Zhao Y, Li J, Jin H, Zhao Y, Zhou H (2015) Hydrothermal synthesis of cobalt particles with hierarchy structure and physicochemical properties. Mater Res Bull 72:7–12

[34] Zhao Y, Zhang X, Wang C, Zhao Y, Zhou H, Li J, Jin H (2017) The synthesis of hierarchical nanostructured MoS_2/Graphene composites with enhanced visible-light photodegradation property. Appl Surf Sci 412:207–213